Atmospheric turbulence

JAKOB MANN
DTU Wind Energy
Technical university of Denmark, Denmark
DK-4000 Roskilde

May 31, 2012

1 Introduction

For many civil engineering structures, including wind turbines, dynamic wind loading caused by the atmospheric turbulence is a serious concern for the designer. Gust loading on streamlines bridge decks requires knowledge of the vertical wind field fluctuations not only in one point, but also how the fluctuations are correlated in space (Simiu and Scanlan 1996, Larose and Mann 1998). Also the horizontal components may be of importance in bridge aerodynamics. For dynamical load calculations on a wind turbine, for example at an off-shore location knowledge of all three wind components and their spatial correlations are needed because the gusts are 'sampled' in a complicated way by the sweeping blades. Yet other structures such as tension leg platforms used for extracting oil on deep waters are sensitive to slow variation in the direction of the wind. Thus various engineering structures are sensitive to various components of wind fluctuations at a wide range of frequencies and also to the spatial correlations of these fluctuations.

The spatial structure of turbulence is also important in order to understand how remote sensing instruments such as lidars measure in a turbulent flow fields. That is because the lidar's sampling volume is rather extended and thus very far from the almost point-like measurements of a ultra-sonic anemometer. The description of how lidars measure turbulence may be found in Mann, Cariou, Courtney, Parmentier, Mikkelsen, Wagner, Lindelöw, Sjöholm and Enevoldsen (2009) for a pulsed lidar, or in Sjöholm, Mikkelsen, Mann, Enevoldsen and Courtney (2009) for a continuous wave (cw) lidar.

The purpose of this contribution is to model the *spectral tensor* of neutral atmospheric surface layer turbulence. The spectral tensor contains all information on spectra, cross-spectra and coherences, which usually are the input requested by wind engineers. We also to devise a general algorithm to simulate three-dimensional fields of all three components of the wind velocity fluctuations. Such simulations are particular useful for time domain simulations of gust loading of wind turbines and other structures.

In section 3 Rapid Distortion Theory (RDT) is used to estimate the tendency of shear to make turbulence anisotropic. RDT is a linearization of the Navier–Stokes equations and has as such limited applicability. The influence of the non-linearity is modeled by postulating some limit as to how much shear is allowed to make the turbulence anisotropic. This modelling uses the concept of eddy lifetime. Despite the various assumptions and postulates the tensor model only contains three adjustable parameters: a length scale describing the size of the energy containing eddies, a non-dimensional number used in the parametrization of eddy lifetime, and the third parameter is a measure of the energy dissipation.

These three parameters are estimated by comparing the model to measurements over the sea in section 4. In section 5 the model is compared to various widely used wind engineering spectral formulations. Finally, in section 6 the spectral tensor is used in a numerical algorithm to simulate three-dimensional fields of all three components of the wind vector. This is done by recasting the Fourier representation of the wind field in the discrete wave-vector space, i.e. as a trigonometric series, where the statistics of the random coefficients are determined by the spectral tensor. The method is considerably simpler, faster and in some aspects more physical than many other currently used simulation algorithms. The method is now used in bridge aerodynamics and in load calculations on wind turbines.

Much of the material presented here has previously been reported in Mann (1994) and Mann (1998), and more details on many aspects may be found in these papers. Newer comparison with neutral atmospheric data taken from Risø's test station Høvsøre may be found in Peña, Gryning, Mann and Hasager (2010) and comparison under different atmospheric stabilities are under way.

2 Definitions

The atmospheric turbulent velocity field is denoted by $\tilde{\boldsymbol{u}}(\boldsymbol{x})$, where $\boldsymbol{x} = (x, y, z)$ is a right-handed coordinate system with the x-axis in the direction of the mean wind field and z as the vertical axis. The fluctuations around the mean wind, $\boldsymbol{u}(\boldsymbol{x}) = (u_1, u_2, u_3) = (u, v, w) = \tilde{\boldsymbol{u}}(\boldsymbol{x}) - (U(z), 0, 0)$, are assumed to be homogeneous in space, which is often the case in the horizontal directions but is only a crude approximation in the vertical. Since turbulence over the sea at high wind speeds is primarily shear-generated, the mean wind field is allowed to vary as a function of z. Because of homogeneity, the covariance tensor

$$R_{ij}(\boldsymbol{r}) = \langle u_i(\boldsymbol{x}) u_j(\boldsymbol{x} + \boldsymbol{r}) \rangle \tag{1}$$

is only a function of the separation vector $\boldsymbol{r}$ ($\langle \quad \rangle$ denotes ensemble averaging).

We shall use *Taylor's frozen turbulence hypothesis* to interpret time series as 'space series' and to serve as a 'dispersion relation' between frequency and wave number (Panofsky and Dutton 1984). Therefore, we can suppress the time argument in $\boldsymbol{u}$.

We only aim at modelling the second order statistics of turbulence, such as variances, cross-spectra, etc. For simulation purposes the velocity field is otherwise assumed to be Gaussian (see section 6). It is still not clear how much influence the statistics of third order, such as skewness, has on load calculations.

All second order statistics can be derived from the covariance tensor or its Fourier transform, the spectral tensor:

$$\Phi_{ij}(\boldsymbol{k}) = \frac{1}{(2\pi)^3} \int R_{ij}(\boldsymbol{r}) \exp(-\mathrm{i}\boldsymbol{k}\cdot\boldsymbol{r})\mathrm{d}\boldsymbol{r}, \tag{2}$$

where $\int \mathrm{d}\boldsymbol{r} \equiv \int_{-\infty}^{\infty}\int_{-\infty}^{\infty}\int_{-\infty}^{\infty} \mathrm{d}r_1\mathrm{d}r_2\mathrm{d}r_3$. The spectral tensor is the basis of the Fourier simulation in section 6.

The stochastic velocity field can be represented in terms of a generalized stochastic Fourier-Stieltjes integral:

$$\boldsymbol{u}(\boldsymbol{x}) = \int \mathrm{e}^{\mathrm{i}\boldsymbol{k}\cdot\boldsymbol{x}}\mathrm{d}\boldsymbol{Z}(\boldsymbol{k}), \tag{3}$$

where the integration is over all wave number space. The orthogonal process $\boldsymbol{Z}$ is connected to the spectral tensor by

$$\langle \mathrm{d}Z_i^*(\boldsymbol{k})\mathrm{d}Z_j(\boldsymbol{k})\rangle = \Phi_{ij}(\boldsymbol{k})\mathrm{d}k_1\mathrm{d}k_2\mathrm{d}k_3, \tag{4}$$

which is valid for infinitely small $\mathrm{d}k_i$ and where * denotes complex conjugation (Batchelor 1953).

Is it very difficult to measure the spectral tensor directly. Instead cross-spectra, defined as

$$\chi_{ij}(k_1, \Delta y, \Delta z) = \frac{1}{2\pi}\int_{-\infty}^{\infty} R_{ij}(x, \Delta y, \Delta z)\mathrm{e}^{-\mathrm{i}k_1 x}\mathrm{d}x \tag{5}$$

are often measured, say by two instruments separated by Δy in the horizontal direction perpendicular to the wind and Δz in the vertical, and are used in practical applications. The connection between the components of the spectral tensor and the cross-spectra is

$$\chi_{ij}(k_1, \Delta y, \Delta z) = \int_{-\infty}^{\infty}\int_{-\infty}^{\infty} \Phi_{ij}(\boldsymbol{k})\mathrm{e}^{\mathrm{i}(k_2\Delta y + k_3\Delta z)}\mathrm{d}k_2\mathrm{d}k_3. \tag{6}$$

When the two indices i and j are the same and $\Delta y = \Delta z = 0$ (6) becomes the one-point spectrum $F_i(k_1) = \chi_{ii}(k_1, 0, 0)$. This definition implies that spectra are *two-sided*, i.e. we get the variance by integrating from $-\infty$ to ∞. This convention is used throughout this chapter.

To distinguish between spectra as functions of wave number k_1 $(= 2\pi f/U)$ and frequency f we use F for the former and S for the latter, i.e. $S_i(f)\mathrm{d}f = F_i(k)\mathrm{d}k$.

The *coherence* is defined as

$$\mathrm{coh}_{ij}(k_1, \Delta y, \Delta x) = \frac{|\chi_{ij}(k_1, \Delta y, \Delta z)|^2}{F_i(k_1)F_j(k_1)}, \tag{7}$$

which can be interpreted as a normalized cross-spectrum.

3 Rapid distortion theory

The incompressible Navier-Stokes equation may be written as

$$\frac{\mathrm{D}\boldsymbol{u}}{\mathrm{D}t} + \boldsymbol{u}\cdot\boldsymbol{\nabla}\ \boldsymbol{U} = -\frac{1}{\rho}\boldsymbol{\nabla}\ p + \text{non-lin. and viscous terms}, \tag{8}$$

where p is the pressure, and $\mathrm{D}/\mathrm{D}t \equiv \partial/\partial t + \boldsymbol{U}\cdot\boldsymbol{\nabla}$ is the 'average Lagrangian derivative.' Assuming a linear shear ($\boldsymbol{\nabla}\ \boldsymbol{U}$ constant), taking the curl, and dropping the non-linear and viscous terms we get

$$\frac{\mathrm{D}\boldsymbol{\omega}}{\mathrm{D}t} = \boldsymbol{\Omega}\cdot\boldsymbol{\nabla}\ \boldsymbol{u} + \boldsymbol{\omega}\cdot\boldsymbol{\nabla}\ \boldsymbol{U}, \tag{9}$$

where $\boldsymbol{\Omega}$ and $\boldsymbol{\omega}$ are the mean and the fluctuating part of the vorticity. It is not at all clear that this linearization is permissible. For example, it can be shown that if the curl of (8) is used to estimate the change in mean square vorticity the non-linear terms will dominate the linear. However, Hunt and Carruthers (1990) argue that when used for the calculation of the response of velocity fluctuations ($\boldsymbol{u}$ or R_{ij}) to a sudden application of a large scale shearing or straining motion the linearization (9) is valid.

Physically, the last term on the right hand side of (9) may be interpreted as the stretching of vorticity by the mean shear (see figure 1). The first term is a distortion of the mean vorticity by velocity fluctuations.

In order to solve (9) we have to Fourier transform the equation. In order to do so, it is important to notice that wave fronts are advected by the mean flow i.e.

$$\frac{\mathrm{d}\boldsymbol{k}}{\mathrm{d}t} = -(\boldsymbol{\nabla}\ \boldsymbol{U})\boldsymbol{k}. \tag{10}$$

The solution to this wave front advection equation is

$$\boldsymbol{k}(t) = \exp(-\boldsymbol{\nabla}\ \boldsymbol{U}t)\boldsymbol{k}_0 \tag{11}$$

where exp means the matrix exponential.

For a general linear $\boldsymbol{U}$ (9) does not have analytic solution. However, for many simple situations such as unidirectional shear, non-rotational stretching or compression, etc. such solutions exists (Townsend 1980).

To get the velocity field from the vorticity we shall express $\mathrm{d}\boldsymbol{Z}$ in terms of $\mathrm{d}\boldsymbol{\Omega}$, which is the Fourier transform of $\boldsymbol{\omega}$ defined in parallel to (3):

$$\boldsymbol{\omega}\ = \boldsymbol{\nabla}\ \times \boldsymbol{u} \Rightarrow \mathrm{d}\boldsymbol{\Omega}\ = \mathrm{i}\boldsymbol{k}\times\mathrm{d}\boldsymbol{Z} \Rightarrow -\mathrm{i}\boldsymbol{k}\times\mathrm{d}\boldsymbol{\Omega}\ = \boldsymbol{k}\times(\boldsymbol{k}\times\mathrm{d}\boldsymbol{Z}). \tag{12}$$

Because of the general identity $\boldsymbol{A}\times(\boldsymbol{B}\times\boldsymbol{C}) = \boldsymbol{B}(\boldsymbol{A}\cdot\boldsymbol{C}) - \boldsymbol{C}(\boldsymbol{A}\cdot\boldsymbol{B})$ and that $\boldsymbol{k}\cdot\mathrm{d}\boldsymbol{Z} = 0$ we get

$$-\mathrm{i}\boldsymbol{k}\times\mathrm{d}\boldsymbol{\Omega}\ = -k^2\mathrm{d}\boldsymbol{Z} \Rightarrow \mathrm{d}\boldsymbol{Z} = \mathrm{i}\frac{\boldsymbol{k}\times\mathrm{d}\boldsymbol{\Omega}}{k^2}. \tag{13}$$

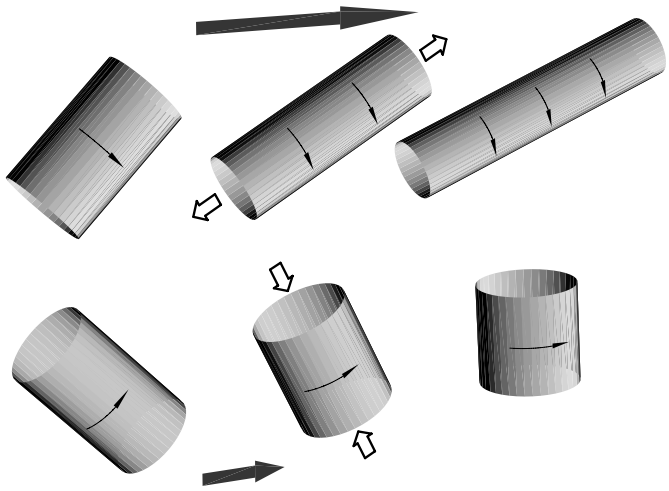

Figure 1: Interpretation of the interplay of shear and turbulence: Two differently oriented eddies are followed over three successive times. Shear stretches (along the axis of rotation) and speeds up the upper eddy while the lower eddy is compressed and slowed down.

We shall re-derive (3.11) in Mann (1994), i.e. set up the equations of motion for

$$\boldsymbol{\nabla}\ \boldsymbol{U} = \begin{pmatrix} 0 & 0 & 0 \\ 0 & 0 & 0 \\ \frac{\mathrm{d}U}{\mathrm{d}z} & 0 & 0 \end{pmatrix}. \tag{14}$$

In this case

$$\boldsymbol{k}(t) = \exp(-\boldsymbol{\nabla}\ \boldsymbol{U}t)\boldsymbol{k}_0 = \begin{pmatrix} 1 & 0 & 0 \\ 0 & 1 & 0 \\ -\frac{\mathrm{d}U}{\mathrm{d}z}t & 0 & 1 \end{pmatrix} \boldsymbol{k}_0, \tag{15}$$

in accordance with (3.13) of Mann, and $\boldsymbol{\Omega} = (0, \mathrm{d}U/\mathrm{d}z, 0)$. The equations of motion (9) becomes

$$\frac{\mathrm{D}\boldsymbol{k} \times \mathrm{d}\boldsymbol{Z}}{\mathrm{D}\beta} = k_2 \mathrm{d}\boldsymbol{Z} + \begin{pmatrix} \mathrm{d}\Omega_3 \\ 0 \\ 0 \end{pmatrix}. \tag{16}$$

Taking the cross product with $\boldsymbol{k}$ and adding $\dot{\boldsymbol{k}} \times (\boldsymbol{k} \times \mathrm{d}\boldsymbol{Z})$ on both sides we get

$$\begin{aligned} -\frac{\mathrm{D}k^2 \mathrm{d}\boldsymbol{Z}}{\mathrm{D}\beta} &= \frac{\mathrm{D}\boldsymbol{k}}{\mathrm{D}\beta} \times (\boldsymbol{k} \times \mathrm{d}\boldsymbol{Z}) + \boldsymbol{k} \times \frac{\mathrm{D}\boldsymbol{k} \times \mathrm{d}\boldsymbol{Z}}{\mathrm{D}\beta} \\ &= \frac{\mathrm{D}\boldsymbol{k}}{\mathrm{D}\beta} \times (\boldsymbol{k} \times \mathrm{d}\boldsymbol{Z}) + k_2 \boldsymbol{k} \times \mathrm{d}\boldsymbol{Z} + \begin{pmatrix} 0 \\ k_3 \\ -k_2 \end{pmatrix} \mathrm{d}\Omega_3. \end{aligned} \tag{17}$$

Writing this more explicitly we get

$$\frac{\mathrm{D}k^2 \mathrm{d}\boldsymbol{Z}}{\mathrm{D}\beta} = \begin{pmatrix} (k_1^2 - k_2^2 - k_3^2)\mathrm{d}Z_3 - 2k_1 k_3 \mathrm{d}Z_1 \\ 2k_1(k_2 \mathrm{d}Z_3 - k_3 \mathrm{d}Z_2) \\ 0 \end{pmatrix} \tag{18}$$

and using $\mathrm{D}k^2/\mathrm{D}\beta = -2k_1 k_3$ from (15) this can be shown to be equivalent to (3.11) in Mann (1994).

The differential equations (18) are easily solved given the initial conditions $\boldsymbol{k}(0) = \boldsymbol{k}_0 = (k_1, k_2, k_{30})$ and $\mathrm{d}\boldsymbol{Z}(\boldsymbol{k}_0, 0)$. Instead of time, t, we shall use the non-dimensional time, β, defined as

$$\beta = \frac{\mathrm{d}U}{\mathrm{d}z}t. \tag{19}$$

The solution to (18) is

$$\mathrm{d}\boldsymbol{Z}(\boldsymbol{k}, \beta) = \begin{bmatrix} 1 & 0 & \zeta_1 \\ 0 & 1 & \zeta_2 \\ 0 & 0 & k_0^2/k^2 \end{bmatrix} \mathrm{d}\boldsymbol{Z}(\boldsymbol{k}_0, 0), \tag{20}$$

where

$$\zeta_1 = \left[C_1 - \frac{k_2}{k_1} C_2 \right] \quad , \quad \zeta_2 = \left[\frac{k_2}{k_1} C_1 + C_2 \right] \tag{21}$$

with

$$C_1 = \frac{\beta k_1^2 (k_0^2 - 2k_{30}^2 + \beta k_1 k_{30})}{k^2 (k_1^2 + k_2^2)} \tag{22}$$

and

$$C_2 = \frac{k_2 k_0^2}{(k_1^2 + k_2^2)^{\frac{3}{2}}} \arctan\left[\frac{\beta k_1 (k_1^2 + k_2^2)^{\frac{1}{2}}}{k_0^2 - k_{30} k_1 \beta}\right]. \tag{23}$$

The equations (15) and (20) give the temporal evolution of individual Fourier modes.

3.1 RDT and surface layer turbulence

In this section we first discuss the connection between RDT and stationary surface-layer turbulence, then the key concept of eddy lifetime, and finally we combine the different parts to obtain the spectral tensor model.

The theory in the previous section describes how turbulence react to a sudden and fast application of a linear shear. It is natural to ask what this has to do with turbulence in the surface layer over the ocean.

If the initial conditions can be represented by the isotropic von Kármán tensor,

$$\Phi_{ij}(\boldsymbol{k}) = \frac{E(k)}{4\pi k^4} \left(\delta_{ij} k^2 - k_i k_j\right), \tag{24}$$

with the energy spectrum

$$E(k) = \alpha \varepsilon^{\frac{2}{3}} L^{\frac{5}{3}} \frac{(Lk)^4}{(1 + (Lk)^2)^{\frac{17}{6}}}, \tag{25}$$

then the tensor $\Phi_{ij}(\boldsymbol{k}, t)$ will become more and more 'anisotropic' with time.

The linearization implied by RDT is unrealistic, and at some point (in time) the stretched eddies will break up. We postulate that eddies of linear dimension $\approx |\boldsymbol{k}|^{-1}$ (or more precisely the Fourier modes) are stretched by the shear over a time which is proportional to their lifetime. The lifetime τ is

$$\tau(k) \propto \varepsilon^{-\frac{1}{3}} k^{-\frac{2}{3}} \tag{26}$$

pertaining, at least in the inertial subrange, to eddies with wave vector magnitude $k = |\boldsymbol{k}|$ (Landau & Lifshitz 1987, § 33).

The basic *postulate* is that the *stationary* spectral tensor

$$\Phi_{ij}(\boldsymbol{k}) \equiv \Phi_{ij}\left(\boldsymbol{k}, \tau(k)\right) \tag{27}$$

describes the surface layer turbulence well. The combination of RDT and scale dependent eddy lifetimes has previously been used by (Derbyshire and Hunt 1993).

Maxey (1982) has described a similar model with the exception that the lifetime τ was assumed to be constant for all wavevectors. ($\tau \mathrm{d}U/\mathrm{d}z$ is called 'the equilibrium value of the effective distortion strain' by Maxey.) Maxey's

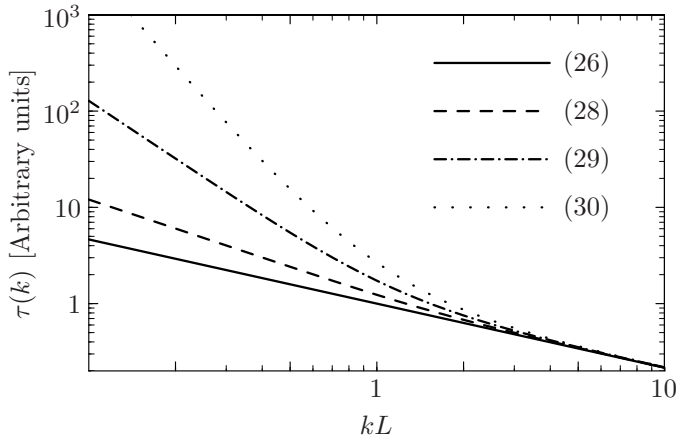

Figure 2: Eddy lifetimes as functions of the magnitude of the wave vector. The lifetimes given by (28) give the most realistic results.

model gives a reasonable, but not perfect, description of the ratios between σ_u^2, σ_v^2, σ_w^2 and $\langle uw \rangle$ for turbulent shear flows. There are, however, two grave drawbacks when the model of Maxey (1982) is used to calculate spectra:

1. The uw-cross-spectrum in the inertial subrange decays as $k_1^{-\frac{5}{3}}$ whereas Wyngaard & Coté (1972) observe and give scaling arguments for $k_1^{-\frac{7}{3}}$.
2. For typical values of the effective distortion strain the model predicts $F_u/F_w \approx 7$ in the inertial subrange whereas it should be $F_u/F_w = \frac{3}{4}$.

The models presented here do not suffer from these shortcomings.

3.2 Eddy lifetimes

At scales larger than the inertial subrange (26) is not necessarily valid. We construct an alternative model for the 'eddy lifetime' assuming that the destruction of an eddy with size k^{-1} is mainly due to eddies comparable to or smaller than k^{-1}. The characteristic velocity of these eddies may be written as $\left(\int_k^\infty E(p)\mathrm{d}p\right)^{\frac{1}{2}}$, and we simply assume the lifetime to be proportional to the size k^{-1} divided by this velocity:

$$\begin{aligned} \tau(k) &\propto k^{-1}\left(\int_k^\infty E(p)\mathrm{d}p\right)^{-\frac{1}{2}} \\ &\propto k^{-\frac{2}{3}}\left[{}_2F_1\left(\frac{1}{3},\frac{17}{6};\frac{4}{3};-(kL)^{-2}\right)\right]^{-\frac{1}{2}} \propto \begin{cases} k^{-\frac{2}{3}} & \text{for } k\to\infty \\ k^{-1} & \text{for } k\to 0 \end{cases} \end{aligned} \quad (28)$$

where we have chosen E as the von Kármán energy spectrum (25) and where ${}_2F_1$ is the hypergeometric function.

Comte-Bellot and Corrsin (1971) give another lifetime model which has the right asymptotic behaviour for $k \to \infty$, the 'coherence-destroying diffusion time' :

$$\begin{aligned} \tau_D(k) &\propto k^{-2}\left[\int_k^\infty p^{-2}E(p)\mathrm{d}p\right]^{-\frac{1}{2}} \\ &\propto k^{-\frac{2}{3}}\left[{}_2F_1\left(\frac{4}{3},\frac{17}{6};\frac{7}{3};-(kL)^{-2}\right)\right]^{-\frac{1}{2}} \propto \begin{cases} k^{-\frac{2}{3}} & \text{for } k\to\infty \\ k^{-2} & \text{for } k\to 0 \end{cases} \end{aligned} \tag{29}$$

which was constructed as the square of the eddy size divided by a k-dependent 'turbulent viscosity'.

Further, the inverse 'eddy-damping rate'

$$\tau_E(k) \propto \left(k^3E(k)\right)^{-\frac{1}{2}} \propto \begin{cases} k^{-\frac{2}{3}} & \text{for } k\to\infty \\ k^{-\frac{7}{2}} & \text{for } k\to 0 \end{cases} \tag{30}$$

is used by Lesieur (1987) in eddy-damped quasi-normal theories of turbulence as a characteristic non-linear relaxation time.

All lifetime models are shown in figure 2 normalized such that they coincide in the inertial subrange. It turns out that σ_u^2 becomes infinite using (29) or (30), while (26) and (28) give reasonable results. It also turns out that the spectra calculated from (28) fit the data better than (26) for which reason (28) is used in the rest of this chapter. Some support for (28) may be found in Panofsky, Larko, Lipschutz, Stone, Bradley, Bowen and Højstrup (1982) who measured eddy 'response times' of eddies in the neutral atmospheric surface-layer. Also Kristensen and Kirkegaard (1987) were in their theoretical model of the growth of a puff in a turbulent fluid compelled to use (28) rather than (29) or (30).

It is convenient to write (28) as

$$\tau(k) = \Gamma\left(\frac{\mathrm{d}U}{\mathrm{d}z}\right)^{-1}(kL)^{-\frac{2}{3}}\left[{}_2F_1\left(\frac{1}{3},\frac{17}{6};\frac{4}{3};-(kL)^{-2}\right)\right]^{-\frac{1}{2}}, \tag{31}$$

where Γ is a parameter to be determined. [1]

It should be emphasized that at low wave numbers the assumptions made so far are not valid. F.ex. the assumptions of linear shear is only valid over small distances, i.e. for large k. Similarly, homogeneity is a dubious assumption for large vertical separations. Finally, despite talking about eddy lifetimes, there is no real modelling of the decay process, because there is no equation describing the non-linear transfer of energy among various wave vectors.

In an attempt to relax the assumption of vertical homogeneity Mann (1994) modelled the influence of the blocking of the surface in addition to shear. This gave slightly better coherence predictions than the present model, but greatly complicated the mathematics and had also other negative consequences.

[1] Keith Wilson has reformulated this expression in terms of the incomplete beta function.

3.3 The uniform shear model

To make a stationary model we use (31) and (27) discussed in the beginning of this section, i.e. we substitute t with τ given by (31). For the 33-component we get

$$\Phi_{33}(\boldsymbol{k}) = \Phi_{33}^{\text{iso}}(\boldsymbol{k}_0)\frac{k_0^4}{k^4} = \frac{E(k_0)}{4\pi k^4}(k_1^2 + k_2^2), \tag{32}$$

where Φ_{33}^{iso} refers to the isotropic von Kármán tensor and E to the energy spectrum (25). The other components become

$$\Phi_{11}(\boldsymbol{k}) = \frac{E(k_0)}{4\pi k_0^4}\left(k_0^2 - k_1^2 - 2k_1k_{30}\zeta_1 + (k_1^2 + k_2^2)\zeta_1^2\right) \tag{33}$$

$$\Phi_{22}(\boldsymbol{k}) = \frac{E(k_0)}{4\pi k_0^4}\left(k_0^2 - k_2^2 - 2k_2k_{30}\zeta_2 + (k_1^2 + k_2^2)\zeta_2^2\right) \tag{34}$$

$$\Phi_{12}(\boldsymbol{k}) = \frac{E(k_0)}{4\pi k_0^4}\left(-k_1k_2 - k_1k_{30}\zeta_2 - k_2k_{30}\zeta_1 + (k_1^2 + k_2^2)\zeta_1\zeta_2\right) \tag{35}$$

$$\Phi_{13}(\boldsymbol{k}) = \frac{E(k_0)}{4\pi k_0^2 k^2}\left(-k_1k_{30} + (k_1^2 + k_2^2)\zeta_1\right) \tag{36}$$

and

$$\Phi_{23}(\boldsymbol{k}) = \frac{E(k_0)}{4\pi k_0^2 k^2}\left(-k_2k_{30} + (k_1^2 + k_2^2)\zeta_2\right). \tag{37}$$

The equations (32) to (37) with (31) constitute the Uniform Shear model (US).

These equations have two differences from the expressions of Townsend (1976) for plane shearing of homogeneous turbulence. The first is the elimination of time by (31) and the second and related difference is that we do not use the turbulent viscosity of Townsend, which would make the decay time for all eddies equal, independent of their sizes.

4 Fitting spectra to observations

First the uncertainties on estimated spectra are discussed. Theses are either caused by variations in atmospheric stability, which persists even at high wind speeds ($>$ 16 m/s) over water, or by statistical variations. Secondly, the measured neutral spectra are fitted to the spectral tensor model. Based on this fit the coherences are finally predicted and compared to the measurements.

4.1 Uncertainties on spectra

Often spectra are averaged over, say, n consecutive frequencies or wave numbers to decrease the random error of the estimate. Alternatively, the time series could be divided into n segments of equal duration. Each segment is then Fourier transformed and the spectrum determined as the average of the absolute square of these Fourier transforms. For either definition the statistical uncertainty

on spectral density F calculated from a stationary time series is (under the assumption that the time series is long compared to the time scale of the process)

$$\frac{\sigma(F)}{\langle F \rangle} = \frac{1}{n^{\frac{1}{2}}} \tag{38}$$

(Koopmans 1974, Bendat and Piersol 1986).

Figure 3 shows the result of an analysis of 14 two-hour time series from the Great Belt. The series have mean speeds U between 16 and 20 m/s and the mean directions are within a narrow range around south where there is an uninterrupted fetch over water for at least 20 km.

Assuming the stability to be neutral, the variation of spectral densities should obey (38) and the standard deviation at the lowest wavenumbers should be around 25% and 5% at $k_1 = 0.1$ m^{-1}. The observed rms variations are clearly larger, at least 50% at the lowest frequencies and maybe 20% at higher frequencies. Most noticeably, there are spectra with only 10% of the spectral density of the others.

This variation is due to the stability of the atmosphere not being neutral. The case with suppressed turbulence is slightly stable and has $U = 16$ m/s. From the point of view of aerodynamic loads this may imply enhanced loads on a bridge deck. While the buffeting loads are smaller the loads from vortex shedding can be much larger. Usually vortex shedding from a bridge deck is suppressed or even destroyed by the turbulence in the atmosphere, but if turbulence is absent as in a stably stratified atmosphere (e.g. warm air flowing out over a cold sea) the vortex shedding might be strong. Stable stratification might also alter loads on off-shore wind turbines because of increased shear.

Unstable stratification also alters the spectrum. Though none of the spectra from the Great Belt are obtained under very unstable situations, an analysis of unstable, high-wind spectra on the west coast of Norway indicate that the spectra are mainly enhanced (by more than 100%) at *very* low frequencies ($f <$ 0.02 Hz). These might be relevant for various off-shore production units (Mann 1992).

4.2 Spectral fitting and prediction of coherences

In order to conduct simultaneous measurements of spectra and coherence over the sea a 70 m high mast was erected 40 m from an existing mast on the easterly spit of Sprogø, an island in the midst of the Great Belt separating the two Danish islands Funen and Zealand. A 15 m long horizontal boom was mounted symmetrically at the top of the new mast so that the whole construction has the form of a letter "T". A Kaijo-Denki DAT-300 omni-directional sonic anemometer was installed at each end of the boom and at the top of the old mast, providing 15.0, 32.5 and 47.5 m horizontal separations between the three co-linear instruments. The mast array is shown in figure 5. More details about the experiment including correction for flow distortion by the sonic anemometers may be found in (Mann, Kristensen and Courtney 1991).

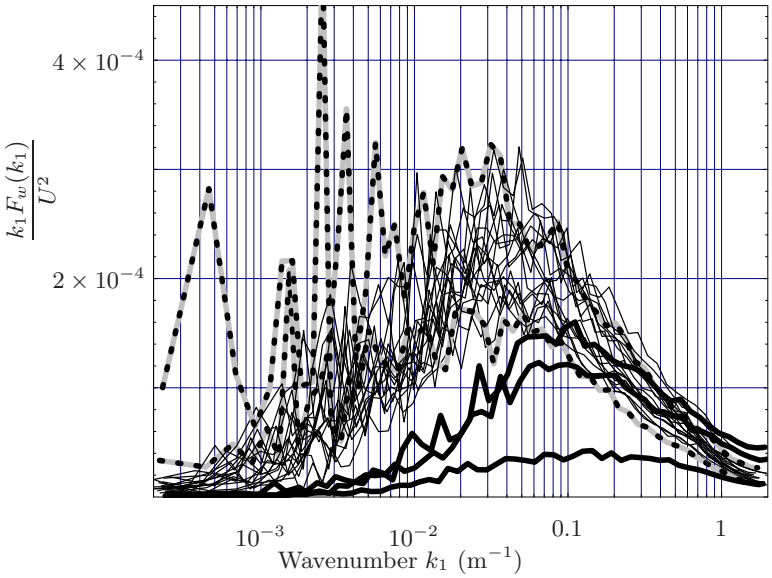

Figure 3: Spectra of w from the Great Belt Coherence Experiment. Mean wind speeds are between 16 and 20 m/s and directions are in a narrow interval around the South. Dashed spectra have slightly unstable stratification, gray have stable, and the thin have neutral.

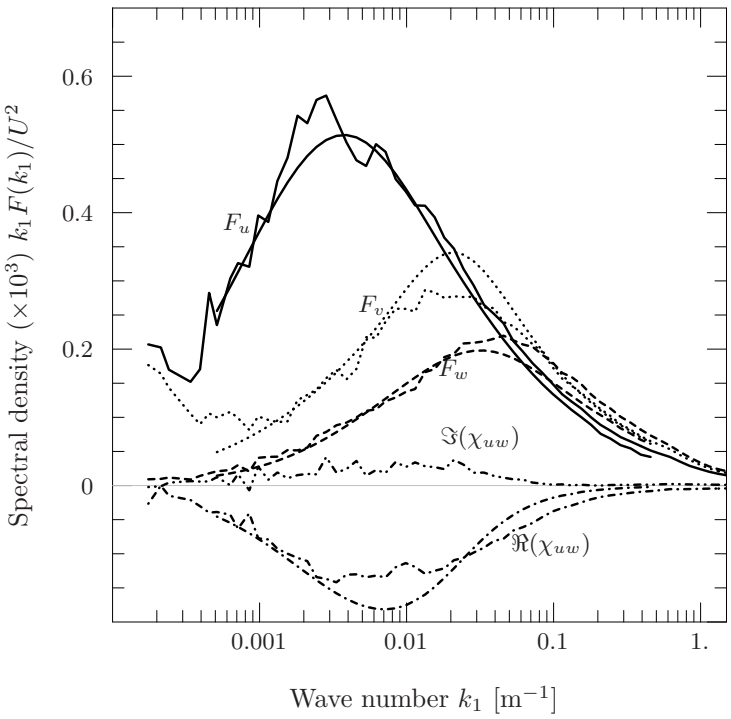

Figure 4: Average u-, v-, w-, and cross-spectra of all the *neutral* runs present in figure 3. The ragged curves are measurements while the smooth are the model spectra. The model has zero imaginary part of the cross-spectrum (quadrature spectrum).

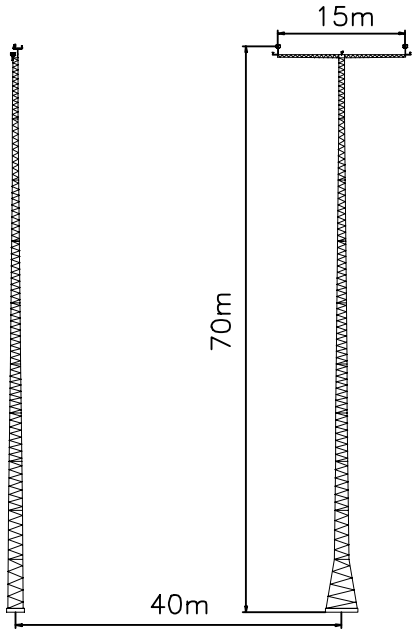

Figure 5: The mast array on Sprogø viewed from SSE. The tiny dots at the top of the masts are the omni-directional sonic anemometers.

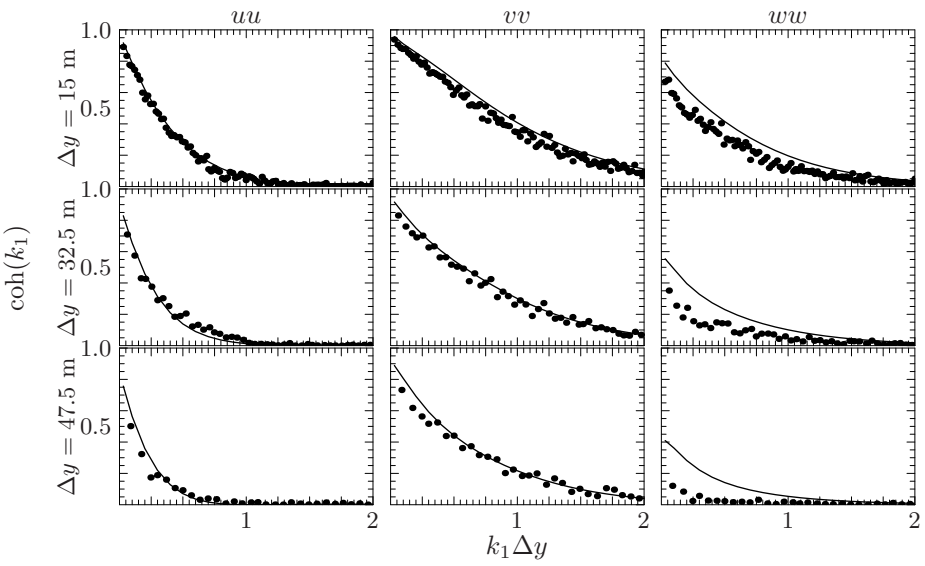

Figure 6: The dots are measured coherences from the same set of data as used for figure 4 for various horizontal separations Δy and for all three velocity components. The lines are the coherences predicted by the model.

The measured spectra shown in figure 4 are an average of 16 *neutral* two hour runs with wind speeds between 16 and 20 m/s. The smooth curves are model spectra derived from the spectral tensor model with the parameters $\Gamma = 3.2$, $L = 61$ m, and $\alpha\varepsilon^{2/3}/U^2 = 1.810^{-4}$ m$^{-2/3}$, which are taken from Mann (1994), who used fewer two hour runs but slightly higher wind speeds.

These parameters are in turn used to predict the coherences as shown in figure 6. As seen from this figure the predictions agree well with the measurements except for the w coherence, especially at the largest separation.

5 Model spectra over the ocean and flat land

Here we compare the tensor model of section 3.1 to spectra and coherences from the literature. We will not give an exhaustive review of spectral models but select a few modern models which the author believes is used in wind engineering. The purpose is to estimate the parameters Γ, L and $\alpha\varepsilon^{2/3}$ for a given mean wind speed U and height above the water surface z.

The logarithmic mean wind profile defines the roughness length:

$$U(z) = \frac{u_*}{\kappa} \ln(z/z_0), \tag{39}$$

where $u_* \equiv (-\langle uw \rangle)^{1/2}_{z\to 0}$ is the friction velocity and $\kappa = 0.40$ the von Kármán constant (Landau and Lifshitz 1987, Panofsky and Dutton 1984).

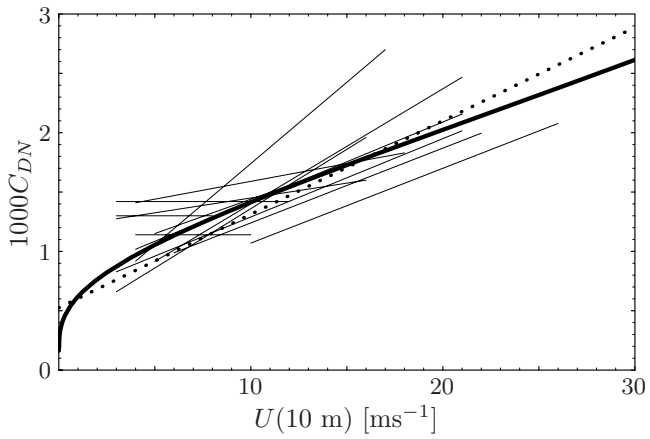

Figure 7: The neutral drag coefficient C_{DN} as a function of mean wind speed at $z = 10$ m. The broad line is from Charnock's relation (41) and (39). The thin lines are empirical relations from (Geernaert 1987) and the dotted line is from NDP (1998), see (50).

ESDU International (1982) gives a slightly more accurate wind profile:

$$U(z) = \frac{u_*}{\kappa}\left(\ln(z/z_0) + 34.5fz/u_*\right) \tag{40}$$

with the Coriolis parameter $f \equiv 2\Omega\sin\phi$, where Ω is the angular velocity in $\text{rad}\,\text{s}^{-1}$ of the Earth and ϕ the geographical latitude. The profile (40) is valid up to $z = 300$ m, below 30 m (39) is a good approximation to (40). Throughout this comparison we use $f = 10^{-4}\ \text{s}^{-1}$.

Charnock (1955) argued that over the sea the roughness length is related to $g = 9.8\ \text{ms}^{-2}$ the acceleration due to gravity and the friction velocity by

$$z_0 = A\frac{u_*^2}{g} \tag{41}$$

where A, the Charnock constant, must be determined experimentally. On basis of an extensive literature study of ocean data Garratt (1977) found that the best fit of (41) is $A = 0.0144$. A slightly newer value is given by ESDU International (1982):

$$A = 0.0167, \tag{42}$$

which will be used here. Over the ocean the neutral drag coefficient

$$C_{DN} = \left(\frac{u_*}{U(10\text{ m})}\right)^2 \tag{43}$$

increases monotonicly with U as can be seen by solving (41) and (39). This is shown in figure 7 as a broad line together with several recent empirical relations.

The figure gives a good impression of the uncertainty in estimates of drag coefficients. Among the various reasons for this variability are atmospheric stability, surface currents, 'wave age', length of the fetch over water, and water depth (Garratt 1977, Geernaert 1987, Brown and Swail 1991). The spectral density of velocity fluctuations is in general proportional to the drag coefficient so the uncertainty of the former is probably of the same order of the latter.

5.1 Code and textbook spectra

Surface layer scaling is used in many spectral models, implying that length scales are proportional to z and that variances are proportional to u_*^2. Therefore, it is convenient to normalize the spectra with u_*^2 and present them as functions of either $n \equiv fz/U$ or $k_1 z$. All spectra in this paper are 'two-sided' implying $\int_\infty^{-\infty} S(f)\mathrm{d}f$ is equal to the variance[2].

The spectra of Kaimal are (Kaimal, Wyngaard, Izumi and Coté 1972, Kaimal and Finnigan 1994)

$$\frac{fS_u(f)}{u_*^2} = \frac{k_1 F_u(k_1)}{u_*^2} = \frac{52.5n}{(1+33n)^{5/3}}, \tag{44}$$

$$\frac{fS_v(f)}{u_*^2} = \frac{8.5n}{(1+9.5n)^{5/3}}, \tag{45}$$

and

$$\frac{fS_w(f)}{u_*^2} = \frac{1.05n}{1+5.3n^{5/3}}. \tag{46}$$

Kaimal's spectra are based on measurements over flat homogeneous terrain in Kansas.

The spectra of Simiu and Scanlan (1996) have the same functional shapes as Kaimal's but the numerical constants are different:

$$\frac{fS_u(f)}{u_*^2} = \frac{100n}{(1+50n)^{5/3}}, \tag{47}$$

$$\frac{fS_v(f)}{u_*^2} = \frac{7.5n}{(1+9.5n)^{5/3}}, \tag{48}$$

and

$$\frac{fS_w(f)}{u_*^2} = \frac{1.68n}{1+10n^{5/3}}. \tag{49}$$

Deviations from surface layer scaling are found in the model spectra from ESDU International (1985). Also the spectra of Norwegian Petroleum Directorate (NDP 1998) and Højstrup, Larsen and Madsen (1990) do not obey surface layer scaling, but they are only limited to u-spectra.

[2]The so-called 'one-sided' spectra, where $\int_0^\infty S(f)\mathrm{d}f$ is equal to the variance, are probably more commonly used.

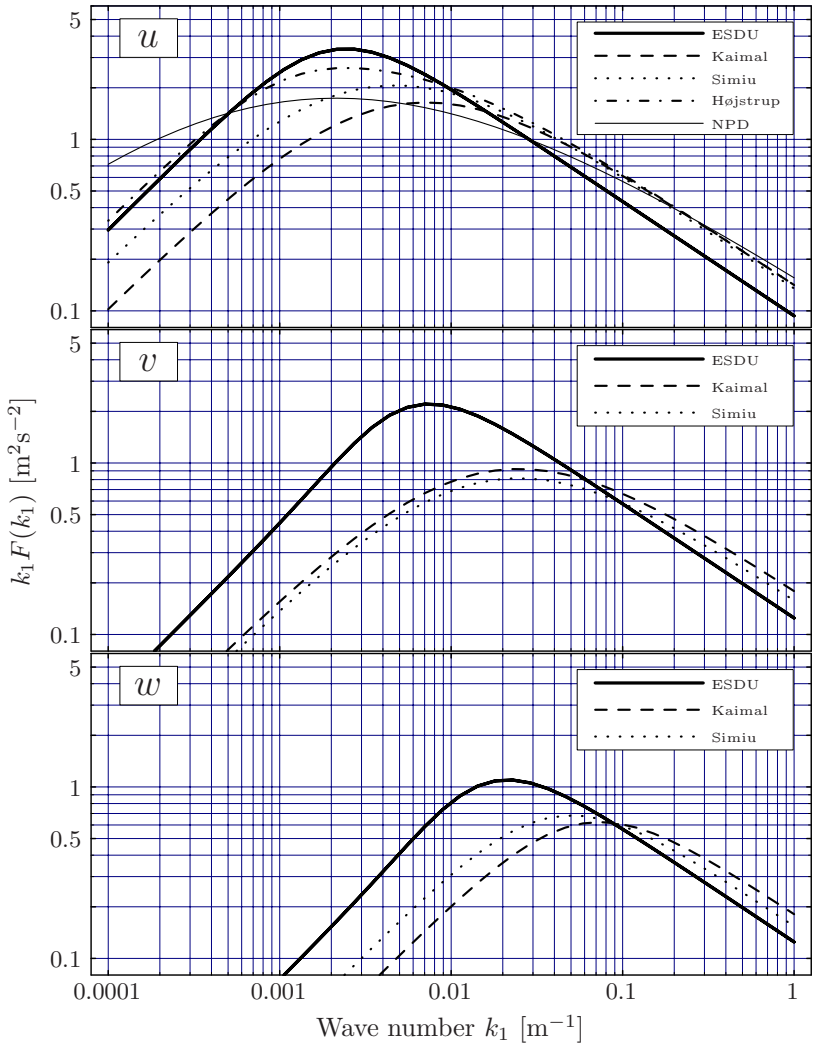

Figure 8: Comparison of spectral models. For the comparison $z = 40$ m and $U = 40$ m/s (over the sea) is chosen. For u ESDU International (1985), (44), (47), (57), (53) are used. For v and w ESDU International (1985), (45) and (48), and ESDU International (1985), (46) and (49), respectively. Eq. (40) together with (41) gives $u_* = 1.78$ m/s and $z_0 = 0.0054$ m.

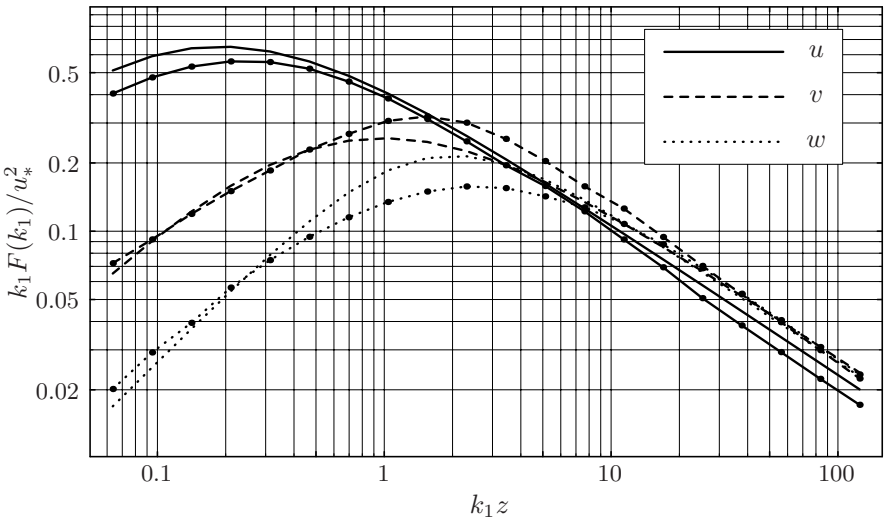

Figure 9: The 'sheared spectral tensor' of section 3.1 (curves with dots) fitted to the models by Simiu and Scanlan (47) – (49). The result is given by (60).

The Engineering Science Data Unit (ESDU) wind profile, spectra and coherences (ESDU International, 1982, 1985 and 1986) are derived from many sources from all over the world during several decades. ESDU proposes that the turbulence intensities and length scales in the surface layer are dependent on mean wind speed. The argument is that the boundary layer depth increases with increasing wind speed implying larger scales of the turbulence. The other models, relying on surface layer scaling do not contain any information on the boundary layer depth and they contain no explicit reference to the mean wind speed. The equations of ESDU are, compared to all other spectral models discussed here, by far the most complicated. Therefore we shall not cite them explicitly. The most important input parameters are, as for the other spectral models, the height above the surface z, and the mean wind speed at some height. Of less important input is the Coriolis parameter which, as mentioned previously, is taken to be $f = 10^{-4}$ s^{-1}. The models we use are valid for the neutral atmosphere.

The u-spectrum of NDP (1998) applies to winds over oceans and assumes the drag coefficient to be

$$C_{DN} = 0.525 \times 10^{-3}(1 + 0.15U_{10}), \tag{50}$$

see figure 7. Integrating $\mathrm{d}U/\mathrm{d}z = u_*/(\kappa z) = \sqrt{C_{DN}}U_{10}/(\kappa z)$ (50) implies that

$$U(z) = U_{10}\left(1 + C\ln\frac{z}{10\text{ m}}\right) \tag{51}$$

with

$$C = 0.0573(1 + 0.15U_{10})^{1/2} \tag{52}$$

where U_{10} has to be measured in meters per second. While discussing the NPD spectrum we also assume the unit of z to be meter, f is Hz and S_u is $\mathrm{m^2 s^{-2} Hz^{-1}}$. The spectral density of the longitudinal wind component is

$$S_u(f) = \frac{160\left(\frac{U_{10}}{10}\right)^2\left(\frac{z}{10}\right)^{0.45}}{\left(1+\tilde{f}^n\right)^{\frac{5}{3n}}} \tag{53}$$

with

$$\tilde{f} = 172 f\left(\frac{z}{10}\right)^{2/3}\left(\frac{U_{10}}{10}\right)^{-3/4} \tag{54}$$

and $n = 0.468$. This spectrum implies that the variance

$$\sigma_u^2 = 0.00309\frac{U_{10}^{2.75}}{z^{0.217}} \tag{55}$$

will decrease with height and not constant as implied by surface layer scaling. Furthermore, the integral length scale

$$\text{length scale} \propto z^{2/3} U_{10}^{1/4} \tag{56}$$

will not be proportional with height but will grow somewhat slower and it will also increase a little with wind speed. This is not consistent with surface layer scaling where it under neutral conditions is constant with wind speed.

Højstrup et al. (1990) suggested that spectra at low frequencies do not obey surface layer scaling because the low frequency part scales with the height of the boundary layer, not z. To verify their model they used data selected for neutrality and high wind speeds ($11 < U < 23$ $\mathrm{ms^{-1}}$) from both over sea and land sites in Denmark. The u-model is[3]

$$\frac{fS_u(f)}{u_*^2} = \left(\frac{2.5n_t}{1+2.2n_t^{5/3}} + \frac{52.5n}{(1+33n)^{5/3}}\right)\frac{1}{1+7.4(z/A)^{2/3}} \tag{57}$$

where the 'neutral length scale' $A = 3000$ m and $n_t = fA/U$. The second term in the parenthesis is the Kaimal spectrum (44).

All spectral model are compared in figure 8 for a specific choice of U and z. Generally, ESDU has larger length scales compared to those by Kaimal and by Simiu & Scanlan, which are similar. NPD and Højstrup support ESDU's large u-scale. ESDU, though, has the most peaked spectra and, at high wave numbers, slightly lower spectral densities. All spectra agree fairly well at high wave numbers but have substantial scatter at low wave numbers.

5.2 Comparison with the spectral tensor model

Here we fit the spectral tensor of section 3.1 to models that describe all three component spectra, namely the ones by Kaimal, Simiu & Scanlan and ESDU.

[3]Højstrup, Larsen and Madsen (1990) also gives a model for the v spectrum, but it was never compared with data, so it will not be discussed here.

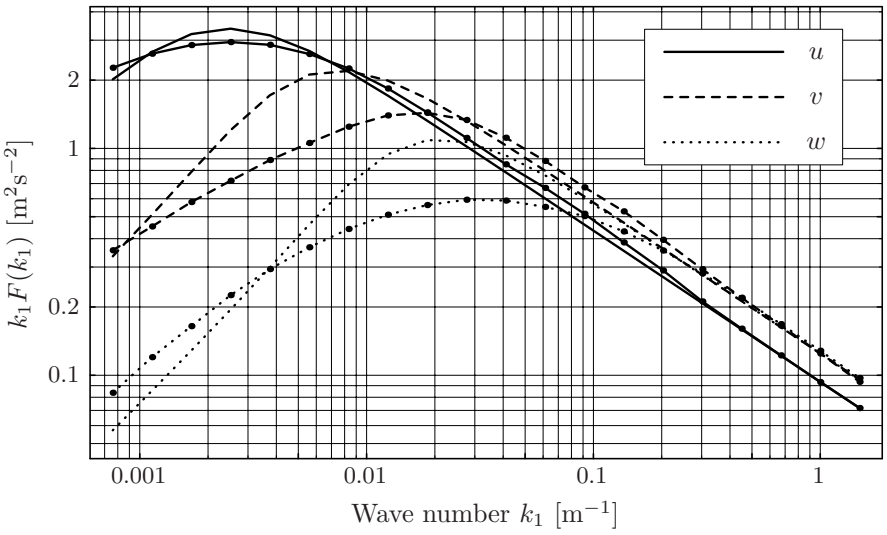

Figure 10: Example with $z = 40$ m and $U = 40$ m/s of the fit of the spectral tensor model (curves with dots) to the ESDU models.

We obtain the parameters Γ, L and $\alpha\varepsilon^{2/3}$ by making a simultaneous least squares fit to the u-, v- and w-model spectra for wave numbers in the range $0.05 < k_1L < 100$. For the Kaimal spectra we get

$$\begin{aligned} \Gamma &= 3.9 \\ L &= 0.59z \\ \alpha\varepsilon^{2/3} &= 3.2\frac{u_*^2}{z^{2/3}}, \end{aligned} \tag{58}$$

where the dependence on z is a consequence of surface layer scaling. For the Simiu & Scanlan spectra, where the fir is shown in figure 9, we get

$$\begin{aligned} \Gamma &= 3.8 \\ L &= 0.79z \\ \alpha\varepsilon^{2/3} &= 2.8\frac{u_*^2}{z^{2/3}} \end{aligned} \tag{59}$$

and for both models u_* can be obtained from figure 7.

It is more complicated to get the parameters from the ESDU models because the spectra no longer depend on U and z in a simple way. For each set $\{U, z\}$, a fit to the tensor model has to be calculated. We do that on a mesh limited by $10 < U < 80$ m/s, $5 < z < 300$ m over the sea. The result is shown in figure 11. As an example of use of these graphs, suppose that the parameters for $U(z = 80 \text{ m}) = 20$ m/s are wanted. From the upper plot of figure 11 we get $L = 33$ m and $\alpha\varepsilon^{2/3} = 0.1$ m$^{4/3}$s^{-2}. The lower plot gives $\Gamma = 4.5$.

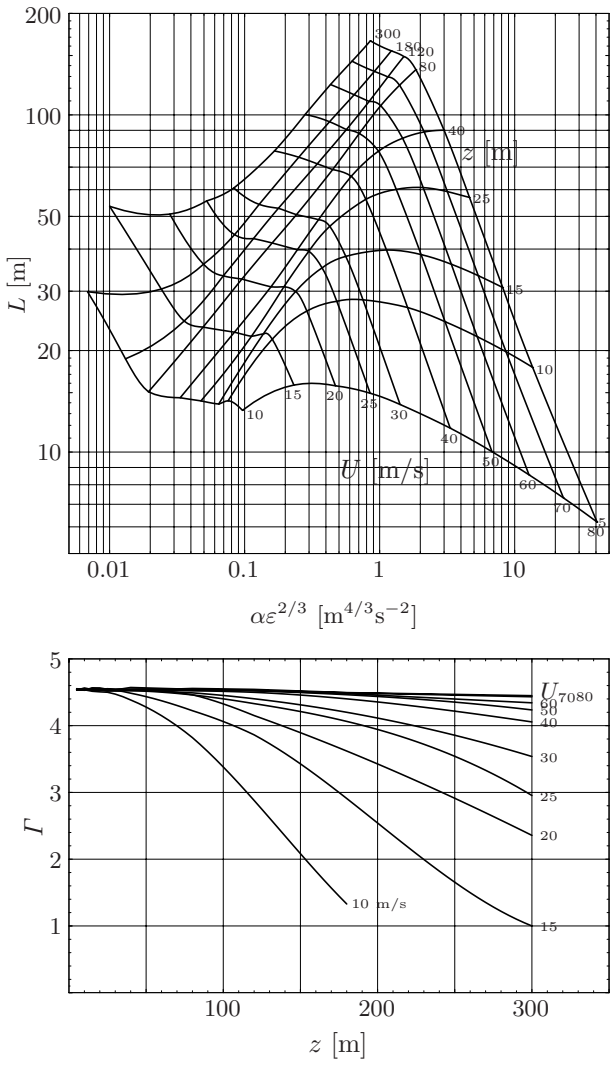

Figure 11: The parameters of the spectral tensor model derived from fits to the ESDU model spectra for turbulence over the sea. Given U and z, all three parameters can be extracted from these plots.

Table 1: Parameters of the spectral tensor derived from different sources for $U(40\text{ m}) = 40$ m/s at sea.

	Γ	L [m]	$\alpha\varepsilon^{2/3}$ [$\text{m}^{4/3}\text{s}^{-2}$]
Great Belt	3.2	35	0.79
Kaimal	3.9	24	0.86
Simiu	3.8	31	0.76
ESDU	4.5	66	0.62

Another example is shown in table 1 where the Great Belt data from (Mann 1994) are extrapolated using neutral surface layer scaling to $U(40\text{ m}) = 40$ m/s. The spectral fit for these values of U and z is shown in figure 10.

Literature coherences and coherences derived from the spectral tensor by (6) and (7) are compared in Mann (1998). Generally, the agreement is good.

6 Wind field simulation

Having discussed the spectral tensor in relation to commonly used literature spectra we now describe how to simulate a velocity field $\boldsymbol{u}(\boldsymbol{x})$, which can be used for calculating loads on engineering structures.

We approximate the integral (3) by a discrete Fourier series:

$$u_i(\boldsymbol{x}) = \sum_{\boldsymbol{k}} \mathrm{e}^{\mathrm{i}\boldsymbol{k}\cdot\boldsymbol{x}} C_{ij}(\boldsymbol{k}) n_j(\boldsymbol{k}), \tag{60}$$

where the l'th component of $\boldsymbol{x}$ is $x_l = n\Delta L_l$ with $n = 1, ..., N_l$. The symbol $\sum_{\boldsymbol{k}}$ denotes the sum over all wave vectors $\boldsymbol{k}$ with components $k_i = m2\pi/L_i$, with the integer $m = -N_i/2, ..., N_i/2$, $n_j(\boldsymbol{k})$ are independent Gaussian stochastic complex variables with unit variance and $C_{ij}(\boldsymbol{k})$ are coefficients to be determined. The great advantage of (60) is that, once the coefficients are known, it can be evaluated very fast by the fast Fourier transform (FFT) (Shinozuka and Deodatis 1991).

Solving (60) we get (approximately, see Mann 1998)

$$C_{ij}(\boldsymbol{k}) n_j(\boldsymbol{k}) = \frac{1}{V(B)} \int_B u_i(\boldsymbol{x}) \mathrm{e}^{-\mathrm{i}\boldsymbol{k}\cdot\boldsymbol{x}} \mathrm{d}\boldsymbol{x}, \tag{61}$$

where $V(B) = L_1 L_2 L_3$ is the volume of B and $\int_B \mathrm{d}\boldsymbol{x}$ means integration over the box B. From (61) it is easy to see that $n_j(\boldsymbol{k})$ *have* to be Gaussian when $u_i(\boldsymbol{x})$ is a Gaussian field. Many authors relax this constraint and let $n_j(\boldsymbol{k})$ have random phase but a fixed absolute value (Shinozuka and Jan 1972, Shinozuka and Deodatis 1991, Shinozuka and Deodatis 1996). Using this approach every sample will get exactly the same variance and, given a wavenumber (or vector), the estimated power spectral density at this wavenumber will be the same for all

realizations of the same process. This might be advantageous in some situations, but it is in contrast to power spectral density estimates of stationary time series which have 100% rms (Press, Flannery, Teukolsky and Vetterling 1992, Bendat and Piersol 1986). The difference between the two approaches is discussed in detail in (Grigoriu 1993). In practice there is little difference and both models could be used. However, the Gaussian approach is usually easier to analyze theoretically and we shall stick to that here.

To find the coefficients $C_{ij}(\boldsymbol{k})$ we calculate the covariance tensor of (61) obtaining

$$\begin{aligned} & C_{ik}^*(\boldsymbol{k})C_{jk}(\boldsymbol{k}) \\ &= \frac{1}{V^2(B)} \int_B \int_B \langle u_i(\boldsymbol{x}) u_j(\boldsymbol{x}') \rangle \, \mathrm{e}^{\mathrm{i}\boldsymbol{k}\cdot\boldsymbol{x}} \mathrm{e}^{-\mathrm{i}\boldsymbol{k}\cdot\boldsymbol{x}'} \mathrm{d}\boldsymbol{x}\mathrm{d}\boldsymbol{x}' \\ &= \frac{1}{V^2(B)} \int \int R_{ij}(\boldsymbol{x}-\boldsymbol{x}') 1_B(\boldsymbol{x}) 1_B(\boldsymbol{x}') \mathrm{e}^{\mathrm{i}\boldsymbol{k}\cdot(\boldsymbol{x}-\boldsymbol{x}')} \mathrm{d}\boldsymbol{x}\mathrm{d}\boldsymbol{x}', \end{aligned} \tag{62}$$

where $1_B(\boldsymbol{x}) = 1$ if $\boldsymbol{x} \in B$ and 0 otherwise. Using the change of variables $\boldsymbol{r} = \boldsymbol{x} - \boldsymbol{x}'$ and $\boldsymbol{s} = \boldsymbol{x} + \boldsymbol{x}'$ having the Jacobian $|\partial(\boldsymbol{r}, \boldsymbol{s})/\partial(\boldsymbol{x}, \boldsymbol{x}')| = 8$ we get

$$C_{ik}(\boldsymbol{k})C_{kj}(\boldsymbol{k}) = \frac{1}{8V^2(B)} \int R_{ij}(\boldsymbol{r}) \mathrm{e}^{-i\boldsymbol{k}\cdot\boldsymbol{r}} \int 1_B\left(\frac{\boldsymbol{s}+\boldsymbol{r}}{2}\right) 1_B\left(\frac{\boldsymbol{s}-\boldsymbol{r}}{2}\right) \mathrm{d}\boldsymbol{s}\mathrm{d}\boldsymbol{r} \tag{63}$$

The inner integration can be carried out according to

$$\int 1_B\left(\frac{\boldsymbol{s}+\boldsymbol{r}}{2}\right) 1_B\left(\frac{\boldsymbol{s}-\boldsymbol{r}}{2}\right) \mathrm{d}\boldsymbol{s} = \begin{cases} \prod_{l=1}^{3} 2(L_l - |r_l|) & \text{for } |r_l| < L_l \text{ for all } l \\ 0 & \text{otherwise} \end{cases} \tag{64}$$

so, using the convolution theorem and noting that the Fourier transform of $L - |r|$ (for $|r| < L$ and else 0) is $L^2 \operatorname{sinc}^2(kL/2)$, we get

$$C_{ik}^*(\boldsymbol{k})C_{jk}(\boldsymbol{k}) = \int \Phi_{ij}(\boldsymbol{k}') \prod_{l=1}^{3} \operatorname{sinc}^2\left(\frac{(k_l - k_l')L_l}{2}\right) \mathrm{d}\boldsymbol{k}', \tag{65}$$

where $\operatorname{sinc} x \equiv (\sin x)/x$. For $L_l \gg L$, the sinc^2-function is 'delta-function-like', in the sense that it vanishes away from k_l much faster than any change in Φ_{ij}, and the area beneath the sinc^2-curve is $2\pi/L_l$. Therefore, we get

$$C_{ik}^*(\boldsymbol{k})C_{jk}(\boldsymbol{k}) = \frac{(2\pi)^3}{V(B)} \Phi_{ij}(\boldsymbol{k}). \tag{66}$$

The solution to (66) is

$$C_{ij}(\boldsymbol{k}) = \frac{(2\pi)^{3/2}}{V(B)^{1/2}} A_{ij}(\boldsymbol{k}) = (\Delta k_1 \Delta k_2 \Delta k_3)^{1/2} \, A_{ij}(\boldsymbol{k}) \tag{67}$$

with $A_{ik}^* A_{jk} = \Phi_{ij}$ and $\Delta k_l = 2\pi/L_l$. This result should be expected when comparing (3) to (60).

Two problems occur by simulating a field by the Fourier series (60) with the coefficients (67). The first is that for many applications the dimensions of the simulated box of turbulence need *not* to be much larger than the length scale of the turbulence model L. Therefore (66) may not be a good approximation to (65). The second problem is that the simulated velocity field (60) is periodic in all three directions. Both problems have been addressed in Mann (1998).

The algorithms above simulate a three-dimensional vector field on a three-dimensional domain, but it can easily be modified to simulate one- or two-dimensional vectors in a 2- or 3-D domain (see Mann 1998). The algorithms are not needed for a one-dimensional domain, i.e. simulation of wind fluctuations in one point as a function of time.

The implementation of the model includes three steps:

1. Evaluate the coefficients $C_{ij}(\boldsymbol{k})$, either by (67) or a modification of this (see Mann 1998).

2. Simulate the Gaussian variable $n_j(\boldsymbol{k})$ and multiply.

3. Calculate $u_i(\boldsymbol{x})$ from (60) by FFT.

The time consumption in the first step is proportional to the total number of points $N = N_1 N_2 N_3$ in the simulation. The required time to perform the FFT is $O(N \log_2 N)$ (Press et al. 1992).

In practice, simulating a three-dimensional field, used for load calculations on wind turbines, with millions of velocity vectors takes of the order of a few minutes on a modern pc.

References

Batchelor, G. K.: 1953, *The theory of homogeneous turbulence*, Cambridge University.

Bendat, J. S. and Piersol, A. G.: 1986, *Random data: Analysis and Measurement Procedures*, 2 edn, Wiley-Interscience.

Brown, R. D. and Swail, V. R.: 1991, Over-water gust factors, *Ocean Engng* **18**(4), 363–394.

Charnock, H.: 1955, Wind stress on a water surface, *QJRMS* **81**, 639–640.

Comte-Bellot, G. and Corrsin, S.: 1971, Simple Eulerian time correlation of full- and narrow-band velocity signals in grid generated, 'isotropic' turbulence, *J. Fluid Mech.* **48**, 273–337.

Derbyshire, S. H. and Hunt, J. C. R.: 1993, Structure of turbulence in stably stratified atmospheric boundary layers; comparison of large eddy simulations and theoretical models, *in* S. D. Moobs and J. C. King (eds), *Waves and Turbulence in Stably Stratified Flows*, Clarendon, Oxford, pp. 23–59.

ESDU International: 1982, *Characteristics of wind speed in the lower layers of the atmosphere near the ground: strong winds (neutral atmosphere)*, ESDU International, London.

ESDU International: 1985, *Characteristics of atmospheric turbulence near the ground. Part II: single point data for strong winds (neutral atmosphere)*, ESDU International, London.

Garratt, J. R.: 1977, Review of drag coefficients over oceans and continents, *Monthly Weather Review* **105**, 915–929.

Geernaert, G. L.: 1987, On the importance of the drag coefficient in air-sea interactions, *Dynamics of Atmospheres and Oceans* **11**, 19–38.

Grigoriu, M.: 1993, On the spectral representation method in simulation, *Probabilistic Engineering Mechanics* **8**, 75–90.

Højstrup, J., Larsen, S. E. and Madsen, P. H.: 1990, Power spectra of horizontal wind components in the neutral atmospheric boundary layer, *in* N. O. Jensen, L. Kristensen and S. E. Larsen (eds), *Ninth Symposium on Turbulence and Diffusion*, American Meteorological Society, pp. 305–308.

Hunt, J. C. R. and Carruthers, D. J.: 1990, Rapid distortion theory and the 'problems' of turbulence, *J. Fluid Mech.* **212**, 497–532.

Kaimal, J. C. and Finnigan, J. J.: 1994, *Atmospheric Boundary Layer Flows, Their Structure and Measurement*, Oxford University Press, New York.

Kaimal, J. C., Wyngaard, J. C., Izumi, Y. and Coté, O. R.: 1972, Spectral charcteristics of surface-layer turbulence, *Q. J. R. Meteorol. Soc.* **98**, 563–589.

Koopmans, L. H.: 1974, *The Spectral Analysis of Time Series*, Academic Press.

Kristensen, L. and Kirkegaard, P.: 1987, Puff kinematics, *Technical Report R–548*, Risø National Laboratory.

Landau, L. D. and Lifshitz, E. M.: 1987, *Fluid Mechanics*, Pergamon Press.

Larose, G. L. and Mann, J.: 1998, Gust loading on streamlined bridge decks, *Journal of Fluids and Structures* **12**(5), 511–536.

Lesieur, M.: 1987, *Turbulence in fluids*, Martinus Nijhoff Publishers.

Mann, J.: 1992, Investigation of atmospheric low-frequency turbulence over the ocean, *Technical Report I–634(EN)*, Risø National Laboratoty.

Mann, J.: 1994, The spatial structure of neutral atmospheric surface-layer turbulence, *J. Fluid Mech.* **273**, 141–168.

Mann, J.: 1998, Wind field simulation, *Prob. Engng. Mech.* **13**(4), 269–282.

Mann, J., Cariou, J.-P., Courtney, M. S., Parmentier, R., Mikkelsen, T., Wagner, R., Lindelöw, P., Sjöholm, M. and Enevoldsen, K.: 2009, Comparison of 3D turbulence measurements using three staring wind lidars and a sonic anemometer, *Meteorol. Z.* **18**(2), 135–140.

Mann, J., Kristensen, L. and Courtney, M. S.: 1991, The great belt coherence experiment – a study of atmospheric turbulence over water, *Technical Report R–596*, Risø National Laboratory.

Maxey, M. R.: 1982, Distortion of turbulence in flows with parallel streamlines, *J. Fluid Mech.* **124**, 261–282.

NDP: 1998, *Acts, regulations and provisions for the petroleum activities, Vol. 2,,* Norwegian Petroleum Directorate.

Panofsky, H. A. and Dutton, J. A.: 1984, *Atmospheric Turbulence*, John Wiley & Sons, New York.

Panofsky, H. A., Larko, D., Lipschutz, R., Stone, G., Bradley, E. F., Bowen, A. J. and Højstrup, J.: 1982, Spectra of velocity components over complex terrain, *Q. J. R. Meteorol. Soc.* **108**, 215–230.

Peña, A., Gryning, S.-E., Mann, J. and Hasager, C. B.: 2010, and charlotte bay hasager, *J. Appl. Meteor. Climat.* **49**, 792–806.

Press, W. H., Flannery, B. P., Teukolsky, S. A. and Vetterling, W. T.: 1992, *Numerical Recipes*, 2nd edn, Cambridge University Press.

Shinozuka, M. and Deodatis, G.: 1991, Simulation of stochastic processes by spectral representation, *Appl. Mech. Rev.* **44**(4), 191–203.

Shinozuka, M. and Deodatis, G.: 1996, Simulation of multi-dimensional gaussian stochastic fields by spectral representation, *Appl. Mech. Rev.* **49**(1), 29–53.

Shinozuka, M. and Jan, C.-M.: 1972, Digital simulation of random processes and its applications, *Journal of Sound and Vibration* **25**(1), 111–128.

Simiu, E. and Scanlan, R. H.: 1996, *Wind Effects on Structures, 3. ed.*, John Wiley & Sons.

Sjöholm, M., Mikkelsen, T., Mann, J., Enevoldsen, K. and Courtney, M.: 2009, Time series analysis of continuous-wave coherent Doppler lidar wind measurements, *Meteorol. Z* **18**(3), 281–287.

Townsend, A. A.: 1976, *The Structure of Turbulent Shear Flow*, 2nd edn, Cambridge University Press.

Townsend, A. A.: 1980, The response of sheared turbulence to additional distortion, *J. Fluid Mech.* **98**, 171–191.